Available online at www.sciencedirect.com

SciVerse ScienceDirect

Ceramics International 38 (2012) 1515–1521

CERAMICS INTERNATIONAL

www.elsevier.com/locate/ceramint

Visible light induced photocatalytic activity of Nb_2O_5/carbon cluster/Cr_2O_3 composite materials

S. Karuppuchamy [a,b,*], H. Matsui [c], K. Kira [c], M.A. Hassan [a,b], M. Yoshihara [c]

[a] Institute of Bioscience, Universiti Putra Malaysia, 43400 Serdang, Selangor, Malaysia

[b] Department of Bioprocess Technology, Faculty of Biotechnology and Biomolecular Sciences, Universiti Putra Malaysia, 43400 Serdang, Selangor, Malaysia

[c] Department of Applied Chemistry, Faculty of Science and Engineering, Kinki University, 3-4-1, Kowakae, Higashiosaka, Osaka 577-8502, Japan

Received 30 July 2011; received in revised form 15 September 2011; accepted 15 September 2011

Available online 21 September 2011

Abstract

Nano-sized Nb_2O_5/carbon cluster/Cr_2O_3 composite material was prepared by the calcination of $NbCl_5$/chromium acetylacetonate/epoxy resin complex under an argon atmosphere. The Pt-loaded Nb_2O_5/carbon cluster/Cr_2O_3 composite material shows the photocatalytic activity under visible light irradiation. The composite material successfully decomposed the water into H_2 and O_2 in the $[H_2]/[O_2]$ ratio of 2. Electron spin resonance spectral examination suggests a two-step electron transfer in the process of Nb_2O_5 → carbon cluster → Cr_2O_3 → Pt.

Keywords: Nanostructure; Carbon cluster; Semiconductor; Chemical synthesis; Electronic structure

1. Introduction

Charge-separated electron excitation under light irradiation is important for the establishment and/or development of new photo-science in the fields of artificial photosynthesis, solar cell production and so on. Semiconductors and/or modified semiconductors could induce such charge-separated electron excitation under visible light irradiation [1–7]. However, the excitation under the whole range of visible light has not been achieved yet. We assumed that the combination of semiconductors and carbon cluster might give a visible light-sensitive electron excitation with the combined function of a light absorption and electron transfer by carbon cluster and semiconductors, respectively. We considered that such composite materials could be obtained by the calcination of either metal atom–organic moiety hybrid copolymers or metal compound/organic polymer complexes under a reducing atmosphere. We have shown the formation of such composite materials with visible light-sensitive electron excitation abilities [7–17]. We previously reported the preliminary results on the electronic behaviors of Nb_2O_5/carbon cluster/Cr_2O_3 composite material obtained from the calcination of a $Nb(HC_2O_4)_5/CrCl_3$/starch complex [15]. In this work, we have reinvestigated the electronic features of Nb_2O_5/carbon/Cr_2O_3 composite materials denoted as III_c obtained by the calcination of a Nb_2Cl_5/chromium acetylacetonate [abbreviated as Cr(acac)$_3$]/epoxy resin complex (Scheme 1) in detail.

2. Experimental

2.1. Reagents

Commercially available niobium chloride ($NbCl_5$), Cr(acac)$_3$, diglycidyl ether of bisphenol A (DGEBA), phthalic anhydride (PA), 1,1-diphenyl-2-picrylhydrazyl (DPPH), hydrogen hexachloroplatinate hexahydrate $H_2PtCl_6{\cdot}6H_2O$, methylene blue, and citric acid were used.

2.2. Synthesis of complexes Is, IIs and III

A mixture of $NbCl_5$ and/or Cr(acac)$_3$, DGEBA and PA was dissolved in 100 mL of acetone. After the solvent was evaporated, the residues were heated in air atmosphere at 120 °C for 3 h to obtain epoxy resin complexes denoted as $I_{1–5}$,

* Corresponding author at: Institute of Bioscience, Universiti Putra Malaysia, 43400 Serdang, Selangor, Malaysia. Tel.: +60 3 8946 7590; fax: +60 3 8946 7593.

E-mail addresses: skchamy@ibs.upm.edu.my, skchamy@gmail.com (S. Karuppuchamy).

0272-8842/$36.00
doi:10.1016/j.ceramint.2011.09.035

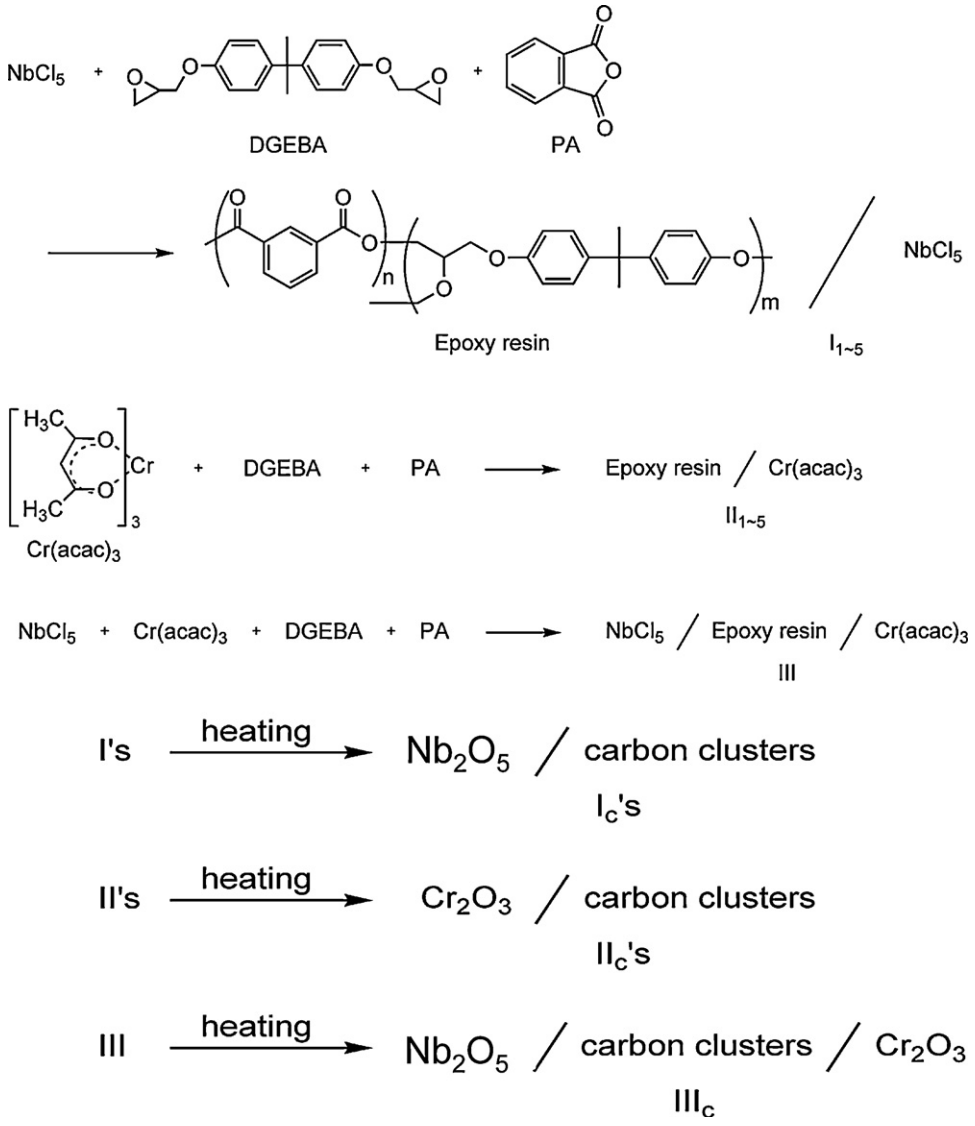

Scheme 1. Schematic explanation for the synthesis of the materials.

$II_{1–5}$ and/or III. The amount of reagents used for the synthesis of complexes is shown in Table 1.

2.3. Calcination of complexes Is, IIs and III

2 g of Is and IIs in a porcelain crucible was heated under an argon atmosphere with a heating rate of 5 °C/min and kept at fixed temperature for 1 h to obtain calcined materials Nb_2O_5/carbon cluster I_cs and Cr_2O_3/carbon cluster II_cs, respectively. The calcination of complex III was also carried out at 500 °C to obtain calcined material Nb_2O_5/carbon cluster/Cr_2O_3 III_{c500}.

2.4. Pt-loading on I_{3c500}, II_{3c500} and III_{c500}

2.4.1. Loading by a photo-electrodeposition procedure

A mixture of 150 mg of I_{3c500}, II_{3c500} and/or III_{c500}, 3.6 mL of an aqueous 2.11 mmol/L hydrogen hexachloroplatinate solution and 3.6 mL of methanol was stirred at room temperature for 1 h under the irradiation of visible light ($\lambda > 460$ nm), and then the precipitates were washed with distilled water and dried under vacuum to obtain Pt-loaded materials $I_{3c500}Pt_{ped}$, $II_{3c500}Pt_{ped}$ and/or $III_{c500}Pt_{ped}$, respectively. Visible light was generated using Hoya-Schott Megalight 100 halogen lamp. The sharp cut filter Y-48 purchased from Hoya Candeo Optronics Co. was used.

Table 1
Charged amounts of reagents for preparing complexes I–III.

Materials	g (mmol)			
	Nb_2Cl_5	$Cr(acac)_3$	DGEBA	PA
I_1	8.96 (33.2)	0	8.75 (25.7)	2.29 (15.4)
I_2	5.77 (21.4)	0	11.3 (33.1)	2.95 (19.9)
I_3	4.26 (15.8)	0	12.5 (36.7)	3.26 (22.0)
I_4	3.37 (12.5)	0	13.2 (38.7)	3.44 (23.2)
I_5	2.79 (10.3)	0	13.6 (40.1)	3.56 (24.1)
II_1	0	16.2 (46.2)	3.05 (8.96)	0.80 (5.38)
II_2	0	9.13 (26.1)	8.62 (25.3)	2.25 (15.2)
II_3	0	6.36 (18.2)	10.8 (31.8)	2.82 (19.1)
II_4	0	4.88 (14.0)	12.0 (35.2)	3.13 (21.1)
II_5	0	3.96 (11.3)	12.7 (37.4)	3.32 (22.4)
III	3.95 (14.6)	5.11 (14.6)	8.68 (25.5)	2.27 (15.3)

2.4.2. Loading by a vacuum evaporation procedure

Pt particles were deposited onto the surface of I_{3c500}, II_{3c500} and III_{c500} (100 mg) by vacuum evaporation treatment using Hitachi Ion Sputter E-1030 with an electric current of 15 mA for 30 min to obtain Pt-loaded materials $I_{3c500}Pt_{ve}$, $II_{3c500}Pt_{ve}$ and $III_{c500}Pt_{ve}$, respectively.

2.5. Characterization

Elemental analysis was performed for C and H with Yanaco MT-6, and for Nb, Cr and Pt by inductively coupled plasma atomic emission spectrometry (ICP-AES) using Shimadzu ICPS-1000 III. Scanning electron microscope–energy-dispersive X-ray spectroscopy (SEM–EDX) analysis was carried out using a Hitachi Hightechnologies S-4800 spectrometer. X-ray photoelectron spectra (XPS) measurements were carried out using Shimadzu ESCA-850. Transmission electron microscopy (TEM) images were observed using Jeol JEM-3010. Electron spin resonance (ESR) spectra measurements were done using Jeol TE-200. Ultraviolet (UV)–visible spectra were measured using a Hitachi U-4000 UV–visible absorption spectrometer. Thermal conductivity detector (TCD) gas chromatography was taken using Shimadzu GC-8A.

The reduction reaction of methylene blue with the calcined materials was performed in the following way. A mixture of 3 mg of the materials and 10 mL of a 0.04 mmol/L methylene blue–0.16 mmol/L citric acid aqueous solution was stirred in the dark for 24 h. The mixture was irradiated with visible light ($\lambda > 460$ nm) for 3 h and the concentration of methylene blue was estimated by UV–vis spectral analysis. The sharp cut filter Y-48 purchased from Hoya Candeo Optronics Co. was used to cut light ($\lambda < 460$ nm). Water photo-decomposition reaction with the calcined materials was carried out in the following way. 10 mg of the materials in 0.1 mL of degassed water was irradiated by visible light ($\lambda > 460$ nm) at room temperature for 12 h under an argon atmosphere, and the evolved H_2 and O_2 gases were analyzed by gas chromatography.

3. Results and discussion

The results of the elemental analysis of complexes I_1–I_5, II_1–II_5 and III are shown in Table 2, indicating that each metal atom was detected in the composite materials. The calcination of I_1–I_5 and II_1–II_5 at fixed temperature gave black-colored materials I_{1c}–I_{5c} and II_{1c}–II_{5c}, respectively.

Table 3 shows the results of the elemental analysis of I_{3c}s and II_{3c}s. The C content ([C]:[metal] ratio) was found to decrease with the increase of the calcination temperature, suggesting that the carbonization of the materials proceeded. The XPS of I_cs and II_cs show the peaks with binding energies at 206.9–207.1 eV due to the $3d_{5/2}$ orbital of Nb atom in Nb_2O_5 [18] and at 586.6–586.9 eV due to the $2p_{1/2}$ orbital of Cr atom in Cr_2O_3 [19], respectively. The TEM observations of the materials showed the presence of particles with the diameters of 1–2 nm, possibly metal oxides, in the carbon phases (Fig. 1). The above results suggest that the calcined materials are composed of nano-sized metal oxides and carbon cluster.

Table 2
Elemental analyses of complexes Is, IIs and III.

Materials	C (%)	H (%)	Nb (%)	Cr (%)	[C]:[metal]
					[C]:[Nb]
I_1	51.9	5.13	17.5	–	23:1
I_2	55.8	5.35	10.4	–	42:1
I_3	57.4	5.58	7.3	–	61:1
I_4	58.7	5.74	5.5	–	83:1
I_5	62.0	5.77	4.7	–	102:1
					[C]:[Cr]
II_1	57.5	6.97	–	11.8	21:1
II_2	65.4	6.98	–	6.8	42:1
II_3	66.2	6.23	–	4.8	59:1
II_4	66.9	6.58	–	3.6	81:1
II_5	67.3	6.21	–	2.9	99:1
					[C]:[Nb]:[Cr]
III	53.7	5.05	7.0	4.1	59:1:1

Table 3
Elemental analyses of calcined materials I_{3c}s and II_{3c}s.

Materials	C (%)	H (%)	Nb (%)	Cr (%)	[C]:[metal]
					[C]:[Nb]
I_{3c500}	62.7	2.2	14.9	–	33:1
I_{3c600}	63.5	1.73	16.2	–	30:1
I_{3c700}	64.0	1.17	17.5	–	28:1
					[C]:[Cr]
II_{3c500}	69.7	2.62	–	9.5	32:1
II_{3c600}	70.3	1.74	–	10.4	29:1
II_{3c700}	72.0	1.18	–	12.5	25:1

The electronic behaviors of calcined materials I_cs and II_cs were examined. First, the ESR spectra measurements of the materials showed a peak signal at 337 mT ($g = 2.003$). Our opinion is that the peak is due to the generation of a free electron on carbon cluster through an electron transfer between carbon cluster and metal oxide particles [8–15]. Similar ESR spectra were observed for other composite materials which are reported earlier [8–15]. The radical spin quantity (*rsq*) of I_{3c}s and II_{3c}s was determined by a double integrating calculation of the differential absorption line with the use of DPPH and the

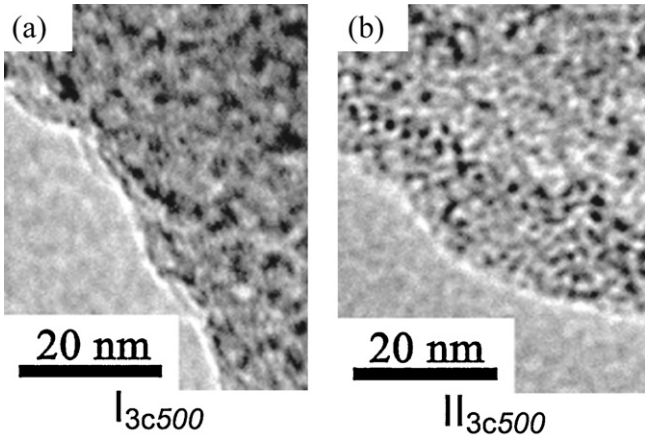

Fig. 1. TEM images of calcined materials: (a) I_{3c500} and (b) II_{3c500}.

Table 4
Radical spin quantities (*rsq*) and reduction activities (*ra*) of I_{3c}s and II_{3c}s.

Materials	*rsq* (spin g^{-1})	*ra* (μmol g^{-1} h^{-1})
I_{3c500}	2.79×10^{20}	5.78
I_{3c600}	1.84×10^{20}	4.49
I_{3c700}	1.23×10^{20}	3.23
II_{3c500}	3.63×10^{19}	2.92
II_{3c600}	1.77×10^{19}	2.12
II_{3c700}	5.49×10^{18}	1.58

results are shown in Table 4. The highest *rsq* values was observed in I_{3c500} for I_{3c}s and II_{3c500} for II_{3c}s, respectively, suggesting that an effective electron transfer may take place in the materials obtained by calcining at 500 °C. Next, the photocatalytic ability of I_{3c}s and II_{3c}s was investigated.

Fig. 2 shows the UV–vis spectral changes of methylene blue in the presence of I_{3c500} under the irradiation of light ($\lambda > 460$ nm). The concentration of methylene blue was found to decrease with the increase of the reaction time, indicating that the material have visible light-responsive reduction ability. The reduction activity (*ra*) of calcined materials I_{3c}s and II_{3c}s was determined by the equation *ra* = (the amount of methylene blue) × (g of the calcined material)$^{-1}$ × (hour)$^{-1}$ and the results are also shown in Table 4. Here again, the highest *ra* values were observed in I_{3c500} for I_{3c}s and II_{3c500} for II_{3c}s, respectively, indicating the occurrence of high catalytic ability in 500 °C-calcined materials. In order to estimate the effect of

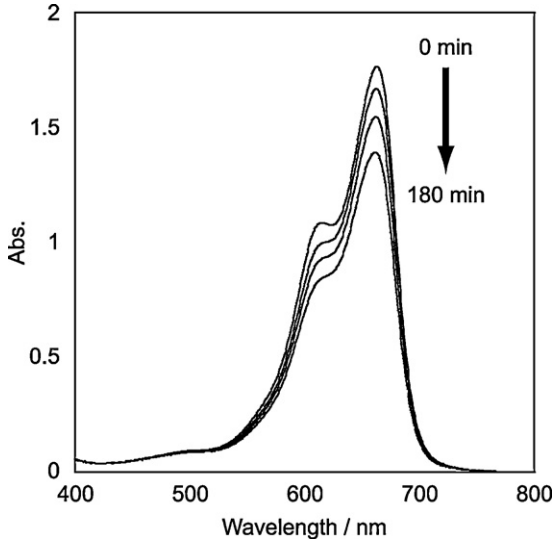

Fig. 2. UV–vis spectra of methylene blue in the presence of I_{3c500} under the irradiation of visible light ($\lambda > 460$ nm).

[C]/[metal] ratios on the electronic natures of the calcined materials, complexes I_1–I_5 and II_1–II_5 were calcined at 500 °C to obtain calcined materials I_{1c500}–I_{5c500} and II_{1c500}–II_{5c500}, respectively, and their *rsq* and *ra* values were determined.

Fig. 3 shows the relationships between the *rsq* values and the [C]/[metal] ratios for either I_{c500}s (Fig. 3a) or II_{c500}s (Fig. 3b), indicating that maximum values were observed at a [C]/[metal]

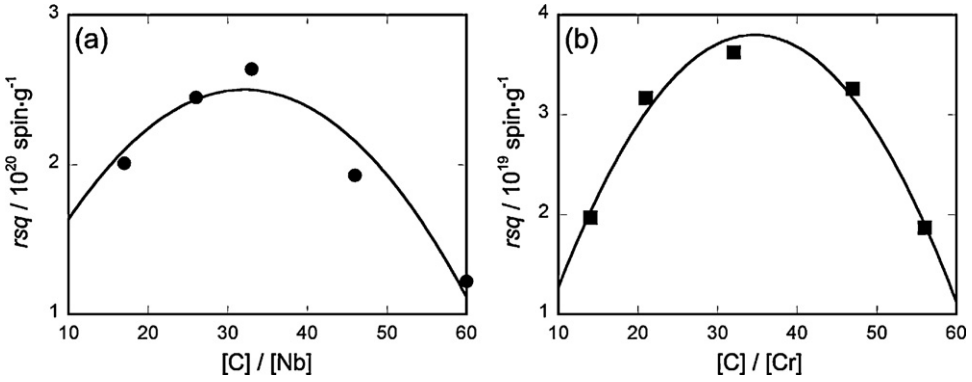

Fig. 3. Relationships between the *rsq* values and the [C]/[metal] ratios for I_{c500}s (a) and II_{c500}s (b).

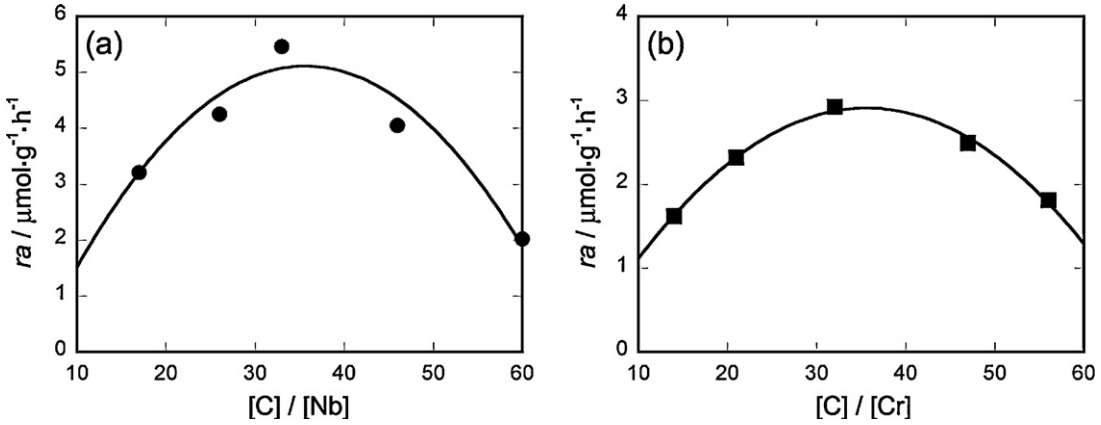

Fig. 4. Relationships between the *ra* values and the [C]/[metal] ratios for I_{c500}s (a) and II_{c500}s (b).

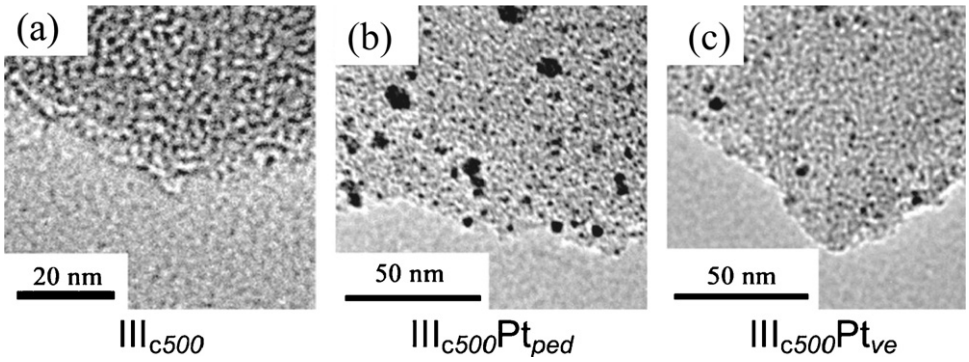

Fig. 5. TEM images of calcined materials: (a) III$_{c500}$, (b) III$_{c500}$Pt$_{ped}$ and (c) III$_{c500}$Pt$_{ve}$.

ratio of ca. 30. The relationships between the *ra* values and the [C]/[metal] ratios are shown in Fig. 4, and again, maximum values were obtained at a [C]/[metal] ratio of ca. 30. These results indicate that a balance between metal oxide and carbon cluster may be important for achieving effective catalytic ability.

The calcination of complex III at 500 °C produced calcined material III$_{c500}$ (C 56.1%, H 2.17%, Nb 12.2%, Cr 6.7%; [C]:[Nb]:[Cr] = 36:1:1). The XPS analysis of III$_{c500}$ showed binding energies at 207.1 eV due to the $3d_{5/2}$ orbital of Nb atom in Nb_2O_5 [18] and at 586.6 eV due to the $2p_{1/2}$ orbital of Cr atom in Cr_2O_3 [19]. The TEM observations revealed the presence of particles with the diameters of 1–2 nm, possibly metal oxides, in the matrix (Fig. 5a). The above results clearly indicate the formation of nano-sized Nb_2O_5/carbon cluster/Cr_2O_3 composite material. The reduction reaction of methylene blue with III$_{c500}$ under visible light ($\lambda > 460$ nm) irradiation was performed to obtain the *ra* value of 11.0 μmol g^{-1} h^{-1}. It is interesting to note that the *ra* value of III$_{c500}$ was higher than the sum (8.7 μmol g^{-1} h^{-1}) of the *ra* values of I$_{3c500}$ and II$_{3c500}$, suggesting that the combination of Nb_2O_5 and Cr_2O_3 in the carbon phases may enhance the photocatalytic ability. In order to examine the electron moving feature of III$_c$, the electron transfer process of I$_{3c500}$ and II$_{3c500}$ was investigated by ESR spectral examination. Fig. 6 shows the ESR spectra of I$_{3c500}$ and II$_{3c500}$ in the presence of either an oxidant (naphthoquinone) or a reductant (1,4-hydroquinone) under the irradiation of visible light ($\lambda > 460$ nm). The signal intensity of I$_{3c500}$ (Fig. 6a) was found to decrease with the addition of the oxidant but increase with the addition of the reductant, indicating that the signal is due to a cation radical.

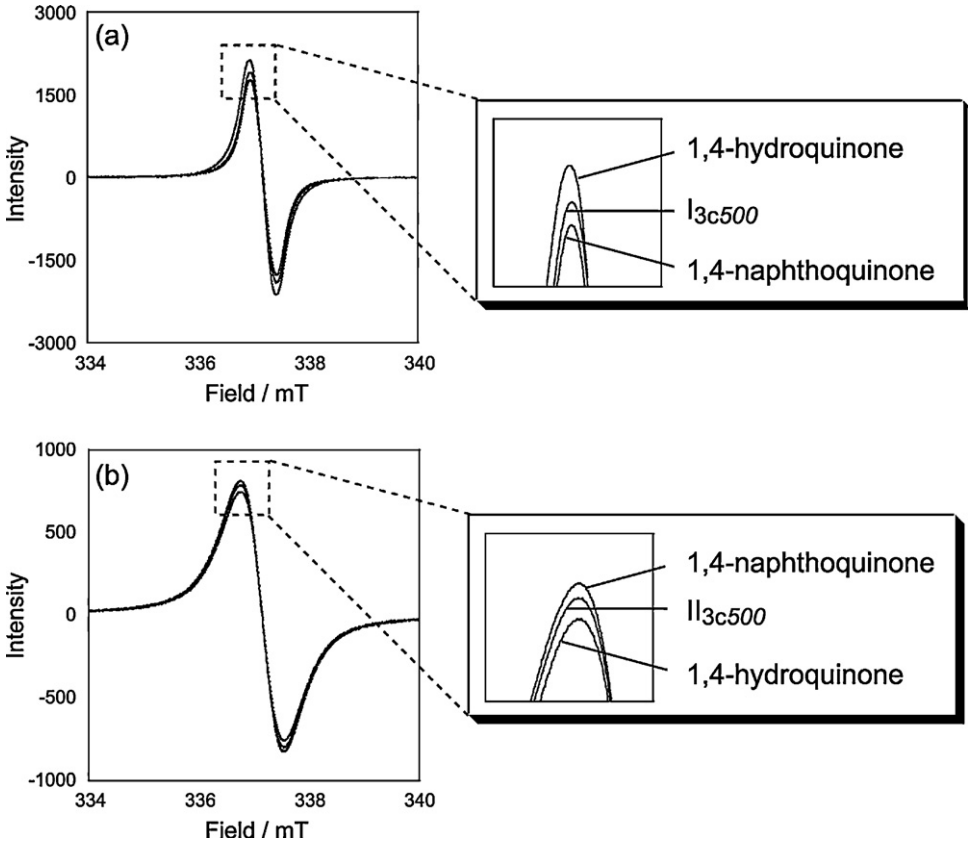

Fig. 6. ESR spectra of I$_{3c500}$ (a) and II$_{3c500}$ (b) in the presence of 1,4-naphthoquinone and 1,4-hydroquinone under the irradiation of visible light ($\lambda > 460$ nm).

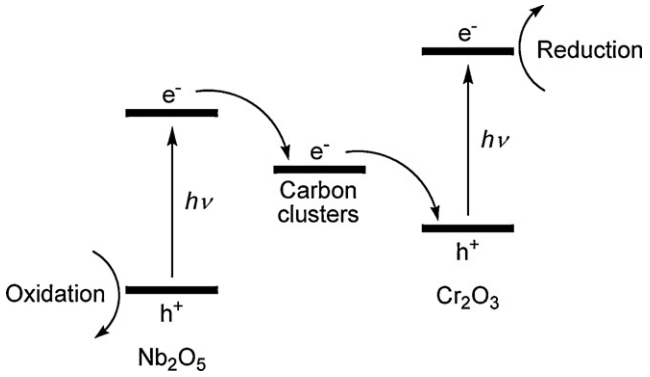

Fig. 7. Schematic diagram for the plausible electron transfer process of III_c.

It is thus deduced that an electron transfer from carbon cluster to Nb_2O_5 parts took place. On the other hand, the peak intensity of II_{3c500} increases with the addition of the oxidant and decreases with the addition of the reductant (Fig. 6b), indicating that the peak is due to a radical anion and thus an electron transfer process occur through $Cr_2O_3 \rightarrow$ carbon cluster. Therefore, the electron transfer in III_c may take place through a two-step electron transfer in the process of $Nb_2O_5 \rightarrow$ carbon cluster $\rightarrow Cr_2O_3$, resulting in the formation of an oxidation site at Nb_2O_5 parts and a reduction site at Cr_2O_3 parts (Fig. 7).

We believe that such a two-step electron transfer by the combination of two semiconductors in the carbon phases may enhance the photo-catalytic ability of the material. Repeated experiments in the photo-reduction reaction of methylene blue with III_{c500} were carried out and the results are shown in Table 5. The *ra* values was found to decrease with the increase of the number of repetitions especially the decomposed amount of methylene blue in the 3rd experiment decreases by 40% in comparison with that in the 1st experiment. In order to examine the causes for the decrease of photo-ability, the SEM observation for III_{c500} was performed after the 3rd experiment (Fig. 8). The SEM indicates that the surface of the material was eroded. The erosion could be due to the attack of generated activated species at the reduction site of the surface of III_{c500} and hence the activities of the material reduced. If this is true,

Table 5
Reduction activities (*ra*) of III_{c500}, $III_{c500}Pt_{ped}$ and $III_{c500}Pt_{ve}$ in the repeated examinations of the visible light-irradiated decomposition reaction of methylene blue.

Times	*ra* (μmol/L)		
	III_{c500}	$III_{c500}Pt_{ped}$	$III_{c500}Pt_{ve}$
1st	9.61	10.1	8.59
2nd	8.15	9.98	8.32
3rd	5.89	6.90	8.49

then the erosion of the material could be controlled by loading a reductive metal on the surfaces of III_{c500}. Therefore, in order to investigate the possible reason for the erosion, the surface of III_{c500} was modified with Pt particles by a photo-electrodeposition method described in Section 2.4.1 to obtain Pt-loaded material $III_{c500}Pt_{ped}$. The TEM image observation of $III_{c500}Pt_{ped}$ was found to reveal the presence of highly dispersed Pt particles with the diameters of 1–2 nm on the surface of III_{c500} (Fig. 5b). The XPS of $III_{c500}Pt_{ped}$ showed a peak at 70.9 eV due to the $4f_{7/2}$ orbital of Pt [20]. The elemental analysis of $III_{c500}Pt_{ped}$ gave the Pt content of 0.8 wt%. The reduction reaction of methylene blue with $III_{c500}Pt_{ped}$ was repeatedly carried out and the results are also shown in Table 5. Again, the *ra* value in the 3rd experiment was found to decrease and the decomposed amount of methylene blue in the 3rd experiment decreases by 30% in comparison with that in the 1st experiment. The ICP-AES analysis of $III_{c500}Pt_{ped}$ recovered after the 3rd experiment showed the Pt content of 0.3 wt%, indicating that the Pt content of 0.5 wt% was peeled out. Pt-peeling was also confirmed by TEM analysis. We considered that photo-electrodeposition method could not form a strong bonding between Pt particles and the surface of III_{c500}. Thus, a vacuum evaporation procedure was applied for Pt-loading on III_{c500} according to the procedure described in Section 2.4.2 to obtain Pt-loaded material $III_{c500}Pt_{ve}$. The TEM observation of $III_{c500}Pt_{ve}$ showed the presence of uniformly dispersed Pt-particles with the diameters of 1–2 nm on the surface of matrix (Fig. 5c). The SEM–EDX analysis of $III_{c500}Pt_{ve}$ indicated a

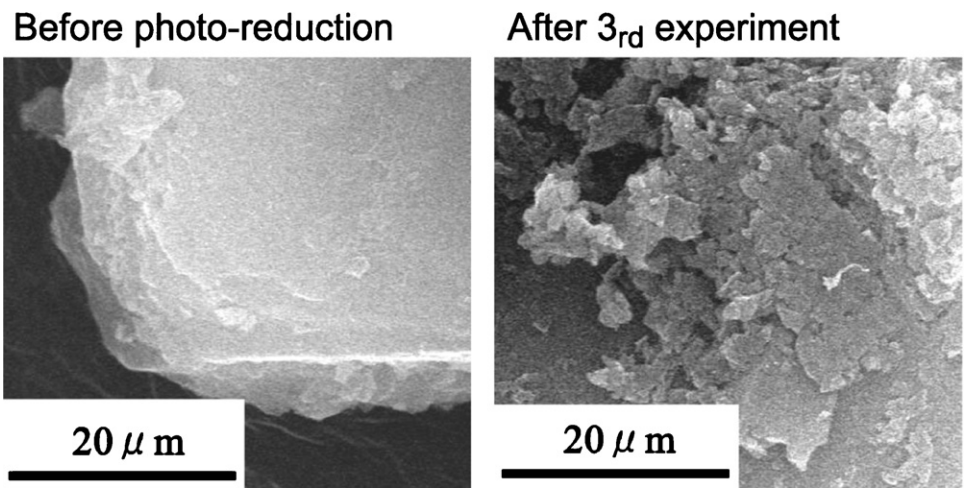

Fig. 8. SEM images of III before and after the photo-reduction of methylene blue.

Table 6
Amounts of H_2 and O_2 evolved in water decomposition reaction with the calcined materials under the irradiation of visible light ($\lambda > 460$ nm).

Materials	nmol		Ratios
	H_2	O_2	$[H_2]:[O_2]$
$I_{3c500}Pt_{ped}$	0	0	
$I_{3c500}Pt_{ve}$	0	0	
$II_{3c500}Pt_{ped}$	0	0	
$II_{3c500}Pt_{ve}$	0	0	
III_{c500}	33	22	1.5:1
$III_{c500}Pt_{ped}$	90	43	2.1:1
$III_{c500}Pt_{ve}$	131	65	2.0:1

peak at 70.9 eV due to the $4f_{7/2}$ orbital of Pt, and elemental analysis showed the Pt content of 1.8 wt%. Repeated experiments of methylene blue decomposition with $III_{c500}Pt_{ve}$ were again performed and the results are also given in Table 5. No variation of the *ra* values was observed for the repeated experiments, and the surface of $III_{c500}Pt_{ve}$ recovered from the methylene blue decomposition experiments was found to be unchanged by SEM–EDX analysis, indicating that an effective Pt-loading was achieved by a vacuum evaporation treatment.

Water splitting experiments with some calcined materials under the irradiation of visible light ($\lambda > 460$ nm) were carried out and the results are shown in Table 6. No H_2 and O_2 evolution was detected for $I_{3c500}Pt_{ped}$, $I_{3c500}Pt_{ve}$, $II_{3c500}Pt_{ped}$ and $II_{3c500}Pt_{ve}$, indicating that the sufficient excitation energy could not be obtained for mono-metal oxide/carbon cluster composite materials to decompose water. On the other hand, the evolution of both H_2 and O_2 gases was observed for III_{c500}, $III_{c500}Pt_{ped}$ and $III_{c500}Pt_{ve}$, indicating that the combination of Nb_2O_5 and Cr_2O_3 in carbon phases caused visible light-sensitive electron excitation which is sufficient to decompose water.

It is noted that the amount of H_2 and O_2 evolved for $III_{c500}Pt_{ped}$ and $III_{c500}Pt_{ve}$ was higher than that for III_{c500}, indicating that the Pt-loading increases the photo-catalytic activity. And it is also noted that the highest H_2 and O_2 evolution was observed for $III_{c500}Pt_{ve}$, indicating that the most effective photo-excitation took place for $III_{c500}Pt_{ve}$. Another interesting observation is that $[H_2]/[O_2]$ ratios for $III_{c500}Pt_{ped}$ and $III_{c500}Pt_{ve}$ were nearly 2, suggesting an occurrence of a smooth two-step electron transfer feature. Meanwhile, a rather small $[H_2]/[O_2]$ ratio was obtained for III_{c500}. Our assumption is that activated species formed at oxidation and/or reduction sites may attack the surface of the material to affect the photo-catalytic activity.

4. Conclusions

We have fundamentally succeeded in constructing an electron transfer system enough to decompose water using Pt-loaded Nb_2O_5/carbon cluster/Cr_2O_3 composite materials under visible light irradiation. We believe that similar photo-sensitive excitation must be achieved by the combination of carbon cluster and a number of photosensitive semiconductors, and our observations will contribute to the development of new photo-science, for example electronic and/or optical device production, artificial photosynthesis, solar cell production, and CO_2 fixation.

References

[1] J. Sato, N. Saito, Y. Yamada, K. Maeda, T. Tanaka, J.N. Kondo, M. Hara, H. Kobayashi, K. Domen, Y. Inoue, RuO_2-loaded β-Ge_3N_4 as a non-oxide photocatalyst for overall water splitting, J. Am. Chem. Soc. 127 (2005) 4150–4151.

[2] M. Matsumura, S. Furukawa, Y. Saho, H. Tsubomura, Cadmium sulfide photocatalyzed hydrogen production from aqueous solutions of sulfite: effect of crystal structure and preparation method of the catalyst, J. Phys. Chem. 89 (1985) 1327–1329.

[3] A. Kudo, Photocatalysis and solar hydrogen production, Pure Appl. Chem. 79 (2007) 1917–1927.

[4] S. Sato, J.M. White, Photodecomposition of water over Pt/TiO_2 catalysts, Chem. Phys. Lett. 72 (1980) 83–86.

[5] J. Yin, Z. Zou, J. Ye, Enhanced photoelectrolysis of water with photoanode Nb:$SrTiO_3$, Appl. Phys. Lett. 85 (2004) 689–691.

[6] A. Kudo, H. Kato, I. Tsuji, Strategies for the development of visible-light-driven photocatalysts for water splitting, Chem. Lett. 33 (2004) 1534–1535.

[7] N. Okada, S. Karuppuchamy, M. Kurihara, An efficient dye-sensitized photoelectrochemical solar cell made from $CaCO_3$-coated TiO_2 nanoporous film, Chem. Lett. (2005) 16–17.

[8] S. Yamamoto, H. Matsui, S. Ishiyama, S. Karuppuchamy, M. Yoshihara, Electronic behavior of calcined material from a tantalum-O-phenylene-S-tin-S-phenylene-O hybrid copolymer, Mater. Sci. Eng. B 135 (2006) 120–124.

[9] T. Furukawa, H. Matsui, H. Hasegawa, S. Karuppuchamy, M. Yoshihara, The electronic behaviors of calcined materials from a (S-nickel-S-phenylene-O)-strontium-(O-phenylene-S-selenium-S) hybrid copolymer, Solid State Commun. 142 (2007) 99–103.

[10] T. Kawahara, T. Kuroda, H. Matsui, M. Mishima, S. Karuppuchamy, Y. Seguchi, M. Yoshihara, Electronic properties of calcined materials from a scandium-O-phenylene-O-yttrium-O-phenylene hybrid copolymer, J. Mater. Sci. 42 (2007) 3708–3713.

[11] T. Kawahara, H. Miyazaki, S. Karuppuchamy, H. Matsui, M. Ito, M. Yoshihara, Electronic nature of vanadium nitride–carbon cluster composite materials obtained by the calcination of oxovanadylphthalocyanine, Vacuum 81 (2007) 680–685.

[12] H. Matsui, S. Yamamoto, T. Sasai, S. Karuppuchamy, M. Yoshihara, Electronic behavior of WO_2/carbon clusters composite materials, Electrochemistry 75 (2007) 345–348.

[13] H. Matsui, S. Karuppuchamy, J. Yamaguchi, M. Yoshihara, Electronic behavior of calcined materials from SnO_2 hydrosol/starch composite materials, J. Photochem. Photobiol. A: Chem. 189 (2007) 280–285.

[14] H. Miyazaki, H. Matsui, T. Nagano, S. Karuppuchamy, S. Ito, M. Yoshihara, Synthesis and electronic behaviors of TiO_2/carbon clusters/Cr_2O_3 composite materials, Appl. Surf. Sci. 254 (2008) 7365–7369.

[15] H. Matsui, K. Kira, S. Karuppuchamy, M. Yoshihara, The electronic behaviors of visible light sensitive Nb_2O_5/Cr_2O_3/carbon clusters composite materials, Curr. Appl. Phys. 9 (2009) 592–597.

[16] S. Ge, H. Jia, H. Zhao, Z. Zheng, L. Zhang, First observation of visible light photocatalytic activity of carbon modified Nb_2O_5 nanostructures, J. Mater. Chem. 20 (2010) 3052–3058.

[17] Y. Zhang, Z. Tang, X. Fu, Y.J. Xu, TiO_2–graphene nanocomposites for gas-phase photocatalytic degradation of volatile aromatic pollutant: is TiO_2–graphene truly different from other TiO_2–carbon composite materials? ACS Nano 4 (2010) 7303–7314.

[18] S. Damyanova, L. Dimitrov, L. Petrov, P. Grange, Effect of niobium on the surface properties of Nb_2O_5–SiO_2-supported Mo catalysts, Appl. Surf. Sci. 214 (2003) 68–74.

[19] D. Park, Y-S. Yun, J.M. Park, XAS and XPS studies on chromium-binding groups of biomaterial during Cr(VI) biosorption, J. Colloid Interface Sci. 317 (2008) 54–61.

[20] Y. Sun, Y. Wang, J.S. Pan, L. Wang, C.Q. Sun, Elucidating the 4f binding energy of an isolated Pt atom and its bulk shift from the measured surface- and size-induced Pt 4f core level shift, J. Phys. Chem. C 113 (2009) 14696–14701.